Power-based Velocity-domain Variable Structure Passivity Signature Control for Physical Human-(Tele)Robot Interaction

Peter Paik, *Student Member, IEEE,* Smrithi Thudi, and S. Farokh Atashzar*, *Senior Member, IEEE*

***Abstract*—The Excess of Passivity (EoP) of the human biomechanics plays an imperative role in absorbing the interaction energy during physical human-(tele)robot interaction and can be exploited by controllers used for stabilization of human-centered (tele)robotic systems. However, the first generation of nonlinear EoP-based stabilizers loaded the force reflection channel resulting in degradation of the force profile. This will challenge applications that are heavily dependent on the quality of force reflection, such as telerobotic rehabilitation. This paper explores the possibility of developing a nonlinear stabilizer that modifies the reflected velocity to the follower-side operator based on the corresponding EoP map. As an applied benefit in the context of telerehabilitation, the proposed stabilizer does not require information about the EoP of all patients; instead, it would require that for the individual therapist who works with the group of patients. The paper provides the mathematical derivation and stability proof of the nonlinear design of the stabilizer named "power-based velocity-domain variable structure passivity signature control (PV-VSPSC)." The proposed nonlinear stabilizer is evaluated through systematic experiments and systematic grid simulation studies in this paper.**

I. INTRODUCTION

Haptics-enabled teleoperation has attracted a great deal of interest over the last two decades with potential applications in space and deep-sea exploration, material handling in hazardous environments, education, robotic surgery, and, more recently, telerobotic rehabilitation [1]–[4]. Stability and transparency are the two major concerns during the operation of telerobotic systems. The stability of such robotic systems with the human in the loop is of paramount importance since the instability of the device can be unsafe and potentially injure the operator. Factors such as communication delay, hard surface contacts, and relaxed user grasps are known to cause instability in teleoperation systems with haptic feedback [2].

Transparency is a measure of the rendered force fidelity. It is the ability to match the impedance of the environment and the one perceived by the human operator through a teleoperation system by exchanging the force and velocity information across the communication network. Signal distortion and delay affect the transparency and, therefore, the performance of the teleoperation system. In a perfectly transparent system, the force and velocity transmitted across the network are unaltered and equal on both sides of the teleoperation. The main challenge has been the stability of the system in the presence of non-passive components caused by communication delays. Therefore, one primary goal of the research community working on telerobotic systems is to develop controllers that guarantee stability while preserving transparency.

Over the years, several controllers have been designed aiming to address this issue. Passivity-based approaches have been a popular choice for the design of controllers to stabilize the bilateral telerobotic systems exposed to time delays. Initially, Anderson and Spong proposed scattering theory to overcome the loss of stability in the presence of communication time delay [5]. Niemeyer and Slotine extended this work and introduced the classical wave variable method based on the passivity theory. The wave variable approach applies an invertible transformation, converting force and velocity variables into internal wave variables in order to ensure stability while transmitting data across a communication channel with a constant time delay [6]. However, the conventional wave variable approach had drawbacks such as wave reflections and instability due to time-varying delays [7]. Several methods have been proposed in the literature to overcome these challenges. For example, in [8], a scaling-based method has been introduced for the wave variable approach that can guarantee the passivity of the communication channels in the presence of variable time delays. In addition, other efforts have been made to improve the system performance, such as combining RBFN neural network and wave variables to minimize the effects of the communication delay and dynamical uncertainties in the system [9].

One of the most successful examples which can handle variable time delays is the time-domain passivity approach (TDPA) introduced by Ryu & Hannaford in [10]. It consists of a passivity observer (PO) that monitors the generated energy and a passivity controller (PC) that adaptively dissipates the active energy. TDPA was extended in [11] to deal with the issues of varying time delays. The controller was also changed from the energy domain in [11] to the power domain in [12]–[15] to enhance the smoothness of the generated force profiles. The issues of position drift were tackled in [16], [17] for the two-port TDPA approach. In addition, TDPA was generalized for multilateral teleoperation in [18], [19].

There are several other recent applications and advances in the field of passivity-based control, including (a) passivity-based configuration decomposition and control for non-holonomic mechanical systems [20], and (b) passivity-based control for enhancing the stability of robotic systems used in simulating satellite dynamics [21]. Efforts to minimize the conservatism of passivity-based controllers have been an active

Peter Paik is with the Department of Electrical and Computer Engineering, New York University (NYU), New York, NY 11201 USA. Smrithi Thudi was with the Department of Mechanical and Aerospace Engineering, NYU. S. Farokh Atashzar is with the Department of Electrical and Computer Engineering, Mechanical and Aerospace Engineering, Biomedical Engineering, NYU. Atashzar is also with NYU WIRELESS Center and NYU CUSP.

This material is based upon work supported by the US National Science Foundation under grants no #2121391 and #2208189. The work is also partially supported by NYUAD Center for Artificial Intelligence and Robotics (CAIR) award # CG010.

P. Paik and S. Thudi share the first authorship.

* Corresponding Author: S. F. Atashzar (f.atashzar@nyu.edu)

area of research [22]–[25]. For example, transparency degradation has been discussed for direct force-reflecting bilateral teleoperation [25].

The controllers mentioned above, however, do not consider the dynamics of the operator or the environment in a bilateral teleoperation system, which may have an inherent energy absorbing capability that can be exploited to extend the scope of the overall system passivity and therefore minimize the conservatism of the system and eventually, reduce the transparency degradation. In this regard, energy-tank-based stabilizers have been proposed in the literature some time in conjunction with wave variables to stabilize the networked robotic systems. For example, two-port energy tanks have been designed by Stramgioli and Secchi in [26] as a means of communicating passive energy criteria between the environment side and the operator side. Further, Secci proposed admittance-based optimization control through the use of energy tanks [27], [28], and more recent work has been proposed, such as in [29], to guarantee passivity, especially whenever an assigned control task may disrupt the passivity of the system. In addition, Atashzar et al. recently proposed the concept of biomechanical excess of passivity (EoP), which is the knowledge regarding the energetic absorption capability of the human biomechanics (while relaxing any classical assumption on linearity) in [30]–[33]. The EoP is formulated based on the Strong Passivity Control Theorem (SPCT). Based on the overall concept of EoP, the authors have generated a new family of stabilizers that compensates (by modifying the force reflected to the operator) only the excess energy which cannot be absorbed by the user's biomechanics. In this context, the value of EoP quantifies the extent of passivity of human biomechanics and can define an energetic margin that can be exploited to guarantee the stability of the system while allowing for the non-passive energy to flow without excessively degrading the transparency. In our paper, we introduce a new stabilization method that takes into account the excess of passivity of the environment to design a causal controller at the follower side and improve the information flow by reducing energy modulation through the estimation and exploitation of the EoP of the environment in the loop.

In this regard, our team initially formulated the modulated TDPC (M-TDPC) [30], which utilizes an estimate of the minimum EoP. Although this controller significantly improves the performance of the system, when compared with conventional TDPC, the proposed algorithm utilizes only a minimum energy absorption margin. An extended version of M-TDPC was proposed specifically for upper limb systems where the user's hand grasp was correlated to the changes in EoP [31] and used in the design of a new nonlinear control scheme named grasp-based passivity signature control (GPS-C). In [31], we have shown that the grasp-related co-contraction of the muscles can drastically increase the energy absorbability of the biomechanics (in a non-symmetric manner considering different interactive directions), and this information was taken into account when designing the GPS-C stabilizer to further reduce the conservatism of the system.

Recently in [32], the authors proposed the latest version of the EoP-based nonlinear controllers for physical human-robot interaction that was designed based on the concept of windowed energy, which can gradually switch between the pure energy-domain formulation and the pure power-domain formulation while taking into account the excess of passivity of the user's biomechanics.

The above-mentioned advancements have been conducted by our team during the last five years in the context of (tele)robotic rehabilitation when force information is imperative, and the assistive behavior of the robot is theoretically non-passive, resulting in failures of classical controllers. One of the challenges of the above-mentioned EoP-base stabilizers is that they rely on force modulation for dissipating the extra energy and guaranteeing stability. Also, the aforementioned EoP-based stabilizers require the EoP of each patient to be identified and tracked. In this paper, we tackle the above problems by proposing a novel stabilization framework that only requires the EoP of the therapist (reducing the variability and enhancing the practicality) while modifying the exchanged velocity information and securing high force tracking performance.

In this paper, we propose an admittance-type stabilizer, named power-based velocity-domain variable structure passivity signature control (PV-VSPSC), which observes the power at the therapy terminal and modifies the velocity reflected to the therapist if the EoP of the therapist cannot compensate for the excess energy induced into the teleoperation system that may lead to instability. This is the first time that the EoP of the remote operator is utilized to modify the velocity sent to the remote operator. It should be noted that the proposed stabilizer belongs to a large family of passivity-based controllers (such as [10], [11], [26]–[29]), which are designed to guarantee a particular passivity-based stability condition and thus the stability of physical human-(tele)robot interaction (pHRI). This is imperative since the instability of the system can compromise the safety of the user(s) and the robotic system. The safety of a pHRI system depends on various parameters, among which stability is an imperative feature that should not be violated when a human is in physical contact with a robot. The authors have contributed to this family of stabilizers in the past [30]–[33], and in this current paper, we propose a new mathematical derivation of the stability condition and stabilizer, taking into account the corresponding information flow, which does not affect force reflection while stabilizing the system, relaxing several existing simplifying assumptions.

Transferring the stabilizer from the patient terminal to the therapist terminal, as proposed in this paper, has the following advantages: (a) The EoP map of the therapist needs only be generated once using the proposed approach. This is because the therapist's limbs are considered to be healthy and, therefore, relatively stable over time. On the other hand, the biomechanical passivity of a stroke patient changes dynamically as the rehabilitation progresses since it is dependent on several factors like muscle spasticity, muscle strength, and range of motion. Hence, the user-specific EoP map may have to be generated periodically as the rehabilitation progresses. Also, since one therapist provides rehabilitation services to several patients, generating the EoP map of the therapist instead of for each patient can save time and cost and also reduce the stress on the patient's limbs. (b) The force feedback to the

patient encodes the information that the therapist wishes to deliver to the patient to satisfy the required therapeutic task. Altering this force information may diminish the perception of the patient from that prescribed by the therapist and may not derive the expected outcomes. (c) Modulating the velocity perceived by the therapist minimally affects the therapy since healthy operators rely more dominantly on visual feedback than haptic feedback, whereas patients rely heavily on haptic feedback. Additionally, this reduces the physical stress on the therapist.

As a result, there is a need for the design and implementation of a stabilizer that minimizes the pre-operational process for patients, minimizes deviation to the therapeutic force field, and reduces physical fatigue on the therapist. The proposed nonlinear stabilizer designed in this paper addresses the aforementioned design factors and is explained in the upcoming sections.

II. Method

A. The Architecture

Fig. 1 shows the two-channel bilateral teleoperation architecture used in this paper. This is a modified version (proposed by Atashzar [34], [35]) of Lawrence's four Channel Architecture. In the rest of this paper, the terminologies are written considering telerobotic rehabilitation application, for which the patient is located on the leader side (to lead motion generation), and the therapist is located on the follower side (to react to the patient's motion by producing therapeutic forces). The mathematical derivation and details can be directly used in other telerobotic applications where a human operator exists on both sides of the teleoperation. Some examples include mirror rehabilitation for the left, and right hand of the same patient [36]–[38], hand-over-hand telerobotic training between expert and novice surgeons [39], [40], and haptic communication [41], [42].

The motion of the patient applied to the leader robot is transmitted across the communication channel to the follower robot held by the therapist. Due to the closed-loop nature of the interaction, the therapist can intervene by applying assistive/resistive forces, which are transmitted back to the patient over the communication network. In the absence of any delay or non-passivity, the architecture achieves perfect transparency even without a stabilizer ($f_p = f_{th}$, where f_p is the force at the patient-leader side, and f_{th} is the force at the therapist-follower side). Also, under these conditions, the architecture guarantees perfect velocity tracking ($v_p = v_{th}$, where v_p is the velocity at the patient-leader side and v_{th} is the velocity at the therapist-follower side).

However, closed-loop networked (such as internet-based) teleoperation often experiences variable delays due to several factors such as stochastic jitters, variable latency, long communication distance, and communication handshakes in reliable internet protocols such as TCP. It has been shown that constant and variable time delay is a non-passive component that can inject non-passive energy into the system, challenging the stability. Additionally, the therapist can inject additional energy into the system by exerting active forces or motions (assistive therapy), leading to non-passivity. All of these can challenge the stability and highlight the need for active stabilization in order to damp out the excess energies. As mentioned earlier, several techniques have been investigated in the literature to deal with time delays, each proposing a different approach to dissipating the excess energy and suggesting different amounts of energy to be dissipated.

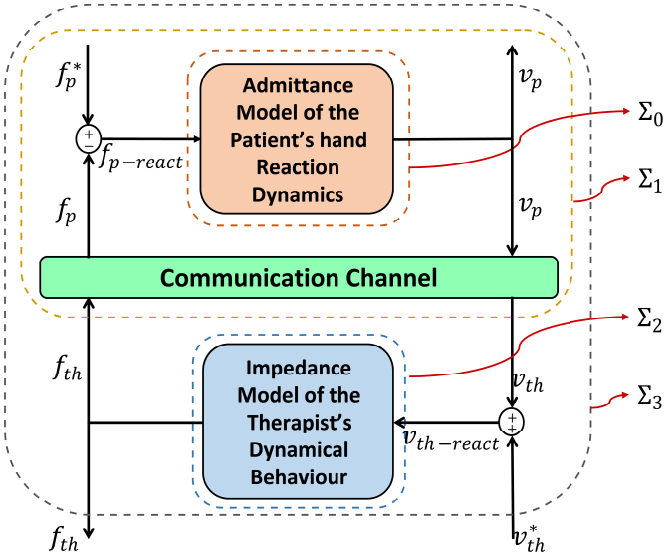

Fig. 1: Closed-loop 2-channel bilateral teleoperation architecture between the admittance based reactive dynamics of the patient terminal and the impedance model of the therapist terminal

Fig. 1, shows the resulting interaction loop of the system. In this figure, $\sum_0$ is the admittance model of the patient-leader terminal, and $\sum_2$ represents the impedance model of the therapist-follower terminal. $\sum_1$ encloses the communication channel and the patient. $\sum_3$ represents the entire teleoperation model.

B. Force and Velocity Decomposition

At the patient terminal, the force is decomposed (as shown in (1)) into an active exogenous component f_p^* which generates deriving force and an impeding reactive component $f_{p-react}$ that resists the robot's motion through spontaneous co-contraction of the muscle and inherent biomechanics.

$$f_p(t) = f_p^*(t) - f_{p-react}(t), \text{ where } f_{p-react} = Z_p(v_p, t) \quad (1)$$

Similarly, at the therapist terminal, the velocity is decomposed into an active component v_{th}^* that applies active motion and a reactive component $v_{th-react}$ that resists the applied forces through spontaneous co-contraction of muscles and inherent biomechanics.

$$v_{th}(t) = v_{th-react}(t) - v_{th}^*(t), \text{ where } v_{th-react} = Y_{th}(f_{th}, t) \quad (2)$$

In (1), $Z_p(v_p, t)$ is the generalized nonlinear impedance model of the patient's reactive dynamics. Likewise, in (2), $Y_{th}(f_{th}, t)$ is the generalized nonlinear admittance model of

the therapist's reactive dynamics. In the literature, a commonly used and relaxed assumption of the user's hand dynamics (which would be equivalent to the patient's hand dynamics in this paper) and environmental dynamics (which would be equivalent to the therapeutic behavior in this context) is a linear second-order mass-spring-damper model [43]–[46]. In order to relax the assumption in this work, we consider an unknown nonlinear and nonautonomous representation for the mentioned models and accordingly do not utilize linear parametrization of the systems. More specifically, the following two points should be highlighted. First, it should be noted that the proposed method does not require any apriori knowledge regarding the patient's hand dynamics. This feature would allow using the proposed system for a wide range of patients (who would have various pathological disorders that would affect their biomechanics) to interact with a therapist. Second, later in this paper, we will discuss the estimation of the excess of passivity of the therapist's biomechanics, which would be the only nonlinear characteristic that will be estimated based on strong passivity theory prior to the operation and will be used intraoperatively when the therapist interacts with any patient.

While the reactive components, i.e., $v_{th-react}$ and $f_{p-react}$ can be modeled as passive systems [31], [33], f_p^* and v_{th}^* which are the active exogenous components (applied by the human to the robot during human-robot interaction) at the patient and therapist terminals can be sources of non-passivity (i.e. excess energy injection). Therefore, this is a potential additional source of non-passivity besides the communication delay, which can cause instability in teleoperation systems. In this work, we do not assume passivity in the generation of exogenous forces by any user of the system.

C. Passivity-based Stability Conditions

In Fig. 1, the system is stable if the entire interconnection $\sum_3$ is passive. This is equivalent to satisfying the following condition based on the strong passivity control theorem (SPCT) [47], [48]:

$$\int_0^t v_{th}^*(\tau)^T.f_{th}(\tau)d\tau \geq 0. \tag{3}$$

Combining (3) with the velocity decomposition equation (2) at the therapist terminal, the stability condition is given as:

$$\int_0^t v_{th-react}(\tau)^T.f_{th}(\tau)d\tau - \int_0^t v_{th}(\tau)^T.f_{th}(\tau)d\tau \geq 0. \tag{4}$$

The definition of the output-passive model (OPM), which can be considered for human biomechanics, is given in (5) based on the SPCT when assuming zero initial condition. Based on SPCT, with zero initial energy condition, the OPM $\forall t \geq 0$:

$$\int_0^t v_{th-react}(\tau)^T.f_{th}(\tau)d\tau \geq \int_0^t \xi_{th}.f_{th}(\tau)^T.f_{th}(\tau)d\tau \tag{5}$$

when $\xi \geq 0$, the system is Output Strictly Passive (OSP) with EoP of ξ. If $\xi < 0$, the system is Output Non-passive (ONP) with Shortage of Passivity (SoP) of ξ.

Since $v_{th-react}$ is not directly accessible during the operation, we can utilize the definition of OPM given in (5) to find a more conservative stability condition based on (4). The new stability condition (6) is calculated by considering the accessible minimal absorption energy of the human biomechanics (i.e. $\int_0^t \xi_{th}.f_{th}(\tau)^T.f_{th}(\tau)d\tau$):

$$\int_0^t \xi_{th}.f_{th}(\tau)^T.f_{th}(\tau)d\tau - \int_0^t v_{th}(\tau)^T.f_{th}(\tau)d\tau \geq 0. \tag{6}$$

If the condition of (6) is met, then the condition of (4) is also met. It can be mentioned that if the power of $\sum_3$ i.e. $v_{th}^*(\tau)^T.f_{th}(\tau)d\tau \geq 0$, then the energy of the terminal which is the accumulation of power over time, $\int_0^t v_{th}^*(\tau)^T.f_{th}(\tau)d\tau$ is also ≥ 0. As a result, the power-based stability condition of (6) is given by:

$$\xi_{th}.f_{th}(\tau)^T.f_{th}(\tau) - v_{th}(\tau)^T.f_{th}(\tau) \geq 0. \tag{7}$$

When this condition is not met, the system is not guaranteed to be passive. (7) represents the energy-based passivity condition that needs to be met to ensure stability. Therefore, a stabilizer, which is discussed later, must be designed to stabilize the interaction.

D. Admittance-based Excess of Passivity

The biomechanical EoP is the inherent ability of the user's biomechanics to absorb kinesthetic energy [31]. Previous studies related to the passivity behavior of the user's biomechanics have shown that the user's biomechanics exhibit strictly dissipative behavior [31], [33] and the corresponding EoP depends on factors such as muscle co-contraction and direction of perturbation. The EoP can be estimated using pre-operative identification to be used in the design of the stabilizer. In [31], an impedance-based EoP was estimated prior to the procedure, and a grasp-based passivity signature (GPS) map was constructed, encoding the effect of directionality and co-contraction (by grasping) on the EoP.

Previous stabilizers developed by Atashzar et al. in [31]–[33] modified the force reflected to the patient's biomechanics to compensate for the compounded non-passive therapeutic energies communicated over the network that cannot be absorbed by the estimated EoP of the patient. This is done to guarantee system stability based on strong passivity theory. However, this method can overload the force reflection gate and over-skew the force information received by the patient.

This paper aims to design and utilize the admittance-based EoP of the therapist instead of the impedance-based EoP of the patient. A novel adaptive nonlinear stabilizer is then developed in this work (as mentioned in Section II.F) which observes the power at the therapist terminal and modifies the velocity reflected to the therapist if the passivity condition, given by (7), is not satisfied, to block only the minimum excess energy that cannot be absorbed in the system. The use of the proposed stabilizer results in minimal adaptive modulation of the motions delivered to the therapist. Thus, it does not affect the therapeutic information context of the force field delivered to the patient. When augmented with visual feedback, this can

be more natural than the force modification counterpart since the stabilizer can reduce the therapist's fatigue, especially for long hours of rehabilitation.

Additionally, using the proposed architecture, the EoP map only needs to be generated once for the therapist instead of pre-determining one for each patient. This can significantly save time and cost, enhance consistency, and reduce the physical and mental loads on the patient, which could have been caused by longer sessions. Also, the EoP map of the patients can differ significantly based on the type of stroke, patient-specific biomechanics, and the stage of rehabilitation. However, calculating the EoP of the therapist will allow us to utilize the same information for a large number of patients.

E. Method for Estimating the EoP of the Therapist

Previously we have developed a protocol to calculate the impedance type interaction in [31]. Here we utilize the same protocol for data collection and will use that in a new mathematical formulation for generating the admittance-type EoP for the therapy terminal needed in this paper.

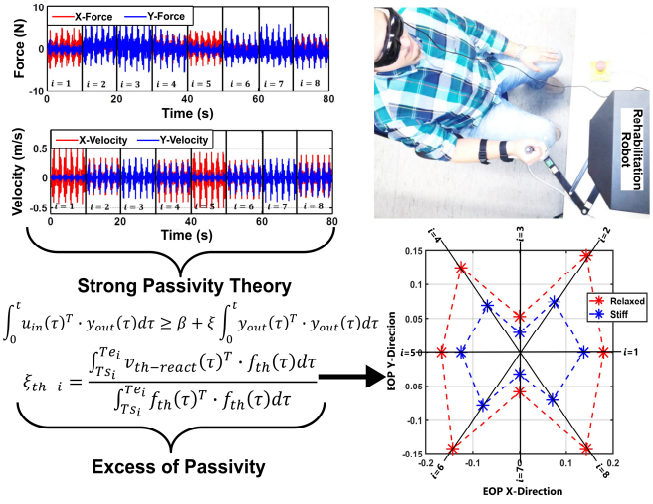

Fig. 2: Experimental Procedure to measure EoP

Regarding the experimental design, it can be mentioned that the user-specific admittance-type EoP map can be estimated by applying multi-frequency directional perturbations to the upper limb of the user when the user is instructed to hold the robot without applying any exogenous velocities such that $v_{th}^* \Rightarrow 0$. The motion profile consists of 10 sinusoids with frequencies ranging from 0 to 2 Hz. The range is considered based on studies on the frequency content of motion during normal daily activities [49], [50]. In order to account for directionality, the robot handle is perturbed in 8 directions ranging from 0 to $7\pi/4$, where each direction is perturbed for 10 seconds for a total time of 80 seconds. The experiment is conducted for two different grasp pressures, namely stiff and relaxed grasps, to show a two-point comparison between their resulting admittance-based EoP. Specifically, a stiff grasp pressure is measured at a grasp pressure close to 80% of the user's maximum grasp pressure and correlates to higher muscle co-contractions, and a relaxed grasp is measured at a grasp pressure close to 5% of the user's maximum grasp pressure and correlates to lower muscle co-contractions. More details on the measurement of grasp pressures can be found in [31]. This experimental setup is shown in Fig. 2. Considering the above design, during the experiment $v_{th-react} = v_{th}$, and since v_{th} is accessible for measurement, the EoP can be calculated from the OPM model (5) as:

$$\xi_{th-i} = \frac{\int_{Ts_i}^{Te_i} v_{th-react}(\tau)^T . f_{th}(\tau)d\tau}{\int_{Ts_i}^{Te_i} f_{th}(\tau)^T . f_{th}(\tau)d\tau}, \tag{8}$$

where ξ_{thi-i} is the admittance-based EoP. Ts_i and Te_i are the starting and ending times of the perturbation in the i^{th} direction. It can be seen that a relaxed grasp results in a higher admittance-based EoP, and a stiff grasp result in a lower admittance-based EoP. This can be explained as such: a relaxed grasp indicates that the human on the environment side, which is the therapist in the context of telerobotic rehabilitation, is holding the robot loosely and responding weakly to the patient's movement. Indeed, if the user at the environment side releases the handle completely, the admittance-based EoP will approach infinity, and thus no velocity will be modified by the proposed stabilizer. As a result of such a situation, no force will be registered on the environment side (since the user released the robot), and thus the patient will experience free motion. On the other hand, during a stiff grasp, the interaction loop between the two users will be high-gain, and in the context of telerehabilitation, it means that the therapist is responding strongly to the patient's motion, increasing the therapeutic force reflection. In this case, the velocity is modified highly by the proposed stabilizer to ensure that the system meets the designed passivity condition. In this paper, a lower-bound on the admittance-based EoP is calculated and used in the stabilizer to be 1/17 m/N.s.

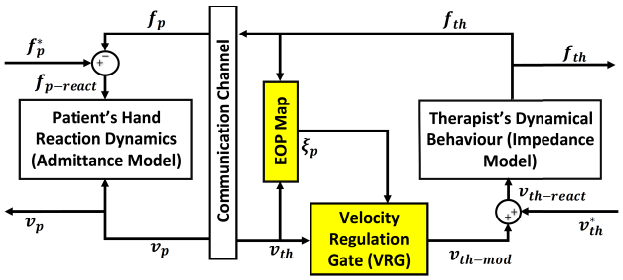

Fig. 3: Velocity-based VSPSC

F. Velocity-based VSPSC - Stabilizer Derivation

The schematic design of the proposed velocity-based VSPSC can be found in Fig. 3. In this design, the therapist's velocity profile is modified by the Velocity Regulation Gate (VRG) based on the following equation:

$$v_{th-mod} = \gamma(t).v_{th}. \tag{9}$$

Here, $\gamma(t)$ is the adaptive scaling factor, ranging from 0 to 1, that needs to be designed as part of the nonlinear stabilizer to ensure the system passivity. In order to generate the design, three separate scenarios are considered based on the passivity condition given in eq. 7.

- **Scenario #1** If $-v_{th}(\tau)^T.f_{th}(\tau) \geq 0$, and since $\xi_{th}.f_{th}(\tau)^T.f_{th}(\tau)$ is always ≥ 0, the passivity condition is satisfied and no modification to the velocity is needed. In summary:

$$\text{If } v_{th}(\tau)^T.f_{th}(\tau) \leq 0, v_{th-mod} = v_{th} \text{ and } \gamma = 1.$$

- **Scenario #2** Otherwise, if the non-passivity of the patient's terminal can be compensated by the reactive dynamics of the therapist terminal, the stability condition given by (7) is satisfied, and thus the complete velocity profile from the patient terminal ($\sum_1$ in Fig. 1) can be reflected to the therapist, as summarized:

$$\text{if } \xi_{th}.f_{th}(\tau)^T.f_{th}(\tau) - v_{th}(\tau)^T.f_{th}(\tau) \geq 0,$$

$$v_{th-mod} = v_{th} \text{ and } \gamma = 1.$$

- **Scenario #3** If the extra energy induced by the patient terminal cannot be compensated for by the EoP of the therapist terminal, then the velocity sent to the therapist must be modified to compensate for the non-passivity to guarantee the stability. As a result, the following design should be considered to impose closed-loop passivity and thus stability:

$$\xi_{th}.f_{th}(\tau)^T.f_{th}(\tau) - v_{th-mod}(\tau)^T.f_{th}(\tau) \geq 0. \quad (10)$$

Substituting (9) in (10), we have:

$$\xi_{th}.f_{th}(\tau)^T.f_{th}(\tau) - \gamma v_{th}(\tau)^T.f_{th}(\tau) \geq 0. \quad (11)$$

From (11), the stability factor γ can be derived as:

$$\gamma \leq \frac{\xi_{th}.f_{th}(\tau)^T.f_{th}(\tau)}{|v_{th}(\tau)^T.f_{th}(\tau)|}. \quad (12)$$

To maximize the transparency, the value of γ is taken to be:

$$\gamma = \frac{\xi_{th}.f_{th}(\tau)^T.f_{th}(\tau)}{|v_{th}(\tau)^T.f_{th}(\tau)|}. \quad (13)$$

As a result, the proposed variable structure passivity design can be summarized as follows.

Considering $v_{th-mod} = \gamma.v_{th}$, where γ is the adaptive velocity modification parameter, the system is passive when:

$$\gamma = \begin{cases} 1 & \text{if } v_{th}(\tau)^T.f_{th}(\tau) \leq 0 \\ 1 & \text{if } \xi_{th} f_{th}(\tau)^T f_{th}(\tau) - v_{th}(\tau)^T f_{th}(\tau) \geq 0 \\ \frac{\xi_{th}.f_{th}(\tau)^T.f_{th}(\tau)}{|v_{th}(\tau)^T.f_{th}(\tau)|} & \text{otherwise} \end{cases} \quad (14)$$

III. Results

The experimental and simulation results for the proposed PV-VSPSC are provided in this Section.

A. Experimental Setup

The system architecture used in the experiment is outlined in Fig. 4. Two Quanser Rehabilitation Robots are utilized; one acts as the leader robot while the other acts as the follower robot. The two robots communicate through UDP communication designed in Simulink. The velocity of the leader robot is sent to the follower robot through the communication, and the force of the follower side is reflected back to the leader robot through the communication using a two-channel optimized telerobotic architecture proposed by our team before [35]. The velocity at the follower side is fed to the proposed control algorithm, which includes a nonlinear Velocity Regulation Gate function that modulates the velocity to guarantee stability. The modified velocity is then sent to the follower robot to be tracked. The positions of the leader (yellow square) and follower (cyan square) are displayed on a graphical user interface (GUI) for each operator, as shown in Fig. 4.

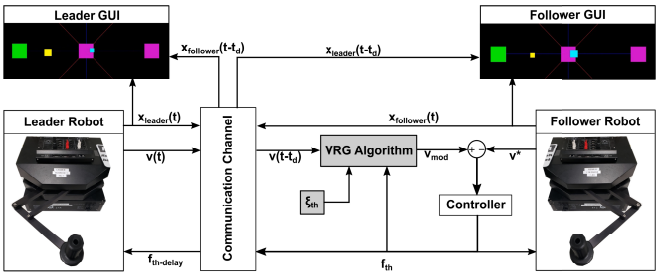

Fig. 4: System Architecture used for the Experiment

For the experiment, the two operators interact using the experimental setup in a point-to-point reaching task. The leader operator is tasked with following the green square on the GUI while the follower operator administers either assistive or resistive interactions. For this, the system would generate an impedance coupling between the two operators. Thus, when the guiding operator leads the motion of the first operator (who is at the leader's side), it results in a guiding force towards the target; likewise, if the guiding operator lags, it results in a damping force away from the target. The experiment is conducted for three different delay values of 0ms, 150ms, and 300ms. In order to show the effects of the stabilizer during resistive therapeutic interaction and assistive therapeutic interaction, the experiment is done in two trials. In the first trial, to mimic resistive therapy, the first user operating the leader robot (the 'patient') drives the motion while the second user operating the follower robot (the 'therapist') resists this motion. In the second trial, the second user assists the movement of the first user by leading the motion, which 'drags' the first user in that direction. A third trial is conducted using a variable delay scenario and compared with the state-of-the-art wave variable with wave scaling method [8]. All three trials are done at the three delay values for 15 seconds each. The experiment is conducted at a sampling frequency of 1kHz.

B. Experimental Results - Trial 1

Fig. 5 shows the associated force, velocity, γ, and stabilizer on/off profiles in the experiment for the first trial when the

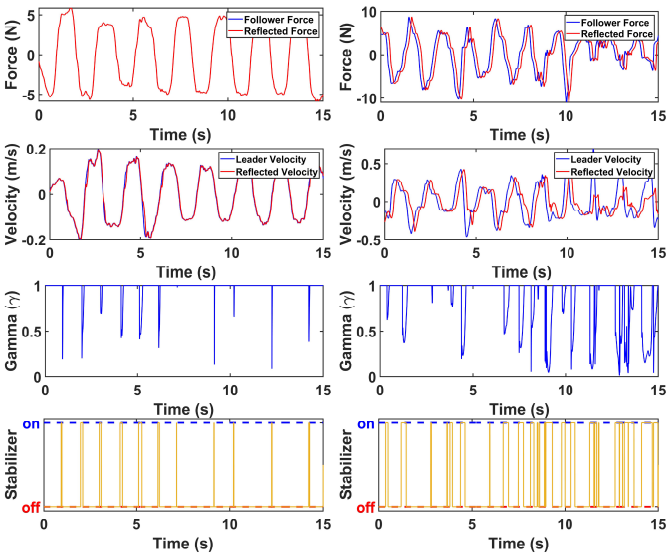

Fig. 5: Force, Velocity, γ, and Stabilizer On/Off profiles with 0ms delay (left) and 150ms delay (right) in trial 1.

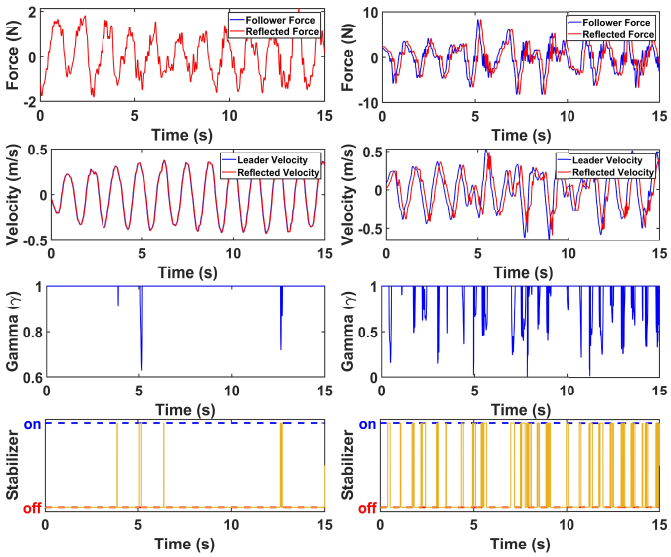

Fig. 6: Force, Velocity, γ, and Stabilizer On/Off profiles with 0ms delay (left) and 150ms delay (right) in trial 2.

delay is set to be 0ms and 150ms. The force profile shows the force that is sent from the follower side (blue) and the force reflected to the leader side (red). The velocity profile shows the velocity sent from the leader side (blue) and the velocity reflected to the follower side after the PV-VSPSC modification (red). The γ profile shows the amount of velocity modification at each time step. And the stabilizer on/off profile shows when the closed loop system approaches non-passivity, according to (7) resulting in activation of the stabilizer. As expected, the follower side forces and reflected forces are tracked well (no force modification, which maximizes force transparency). It should also be noted that during 0ms delay, when the communication does not challenge the passivity of the interaction, using the proposed stabilizer, the velocity tracking experiences minimal-to-no perturbation, as expected based on the design. At 150 ms delay, the amount of velocity modification increases to ensure system passivity and, therefore, stability. The amount of velocity modification is shown in the γ profiles. The stabilizer activates whenever the passivity condition given in (7) is broken and modifies the velocity to ensure that this condition is met; the stabilizer activation profile shows that the stabilizer is much more active at higher delays than at lower delays.

C. Experimental Results - Trial 2

Fig. 6 shows the associated force, velocity, γ, and stabilizer on/off profiles in the experiment for the second trial when the delay is set to be 0ms and 150ms. The force profiles show high force tracking in both resistive and assistive interaction scenarios. As the delay value increases, the amount of velocity modification by the stabilizer also increases, and the stabilizer is able to guarantee stability even though there is more than one source of non-passivity due to the assistive interaction. The stabilizer activates and modifies the velocity whenever the passivity condition (7) is not met. The results from trial 1 and trial 2 show that the stabilizer can handle both passive and non-passive behaviors of the closed-loop system while guaranteeing stability.

Box plot distributions of the absolute force, absolute velocity, and absolute velocity error for trial 1 and trial 2 are shown in Fig. 7 and Fig. 8, respectively. The mean γ for each trial is also provided. Each figure has four subplots (A), (B), (C), and (D). In subplot (A), the blue box plots represent the force distribution at the follower side, and the red box plot represents the reflected force distribution at the leader side. In subplot (B), the blue box plots represent the velocity distribution before the stabilizer, and the red box plots represent the modified velocity distribution after the nonlinear VRG modulation due to the proposed stabilizer. Wilcoxon non-parametric sign rank tests are performed between the forces in subplot (A) and the velocities in subplot (B). Similarly, the sign rank test is performed for the velocity error between delays in subplot (C). Within these plots, 'n.s.' indicates that there is no significant difference between the two distributions ($p > 0.1$), '*' indicates that there is a measurable difference between the two distributions ($p < 0.05$), and '**' indicates that there is a significant difference between the two distributions ($p < 0.001$).

Fig. 7(A) and Fig. 8(A) show the distribution of the follower-side force and distribution of reflected force to the leader side has no significant difference ($p > 0.1$), and this is because the proposed stabilizer applies no force modulation to maximize the quality of force reflection while guaranteeing the stability of the system. Fig. 7(B) and Fig. 8(B) show that the velocity distribution after the stabilizer is lower than the velocity distribution before the stabilizer ($p < 0.001$). This indicates that the VRG-based nonlinear stabilizer is modifying the velocity by dissipating extra energy through the velocity channel to ensure that the system is passive and thus stable. Fig. 7(C) and Fig. 8(C) show the absolute velocity error distribution between the velocities before and after the stabilizer. It is imperative to note that as the delay increases, the velocity error distribution increases ($p < 0.001$). This

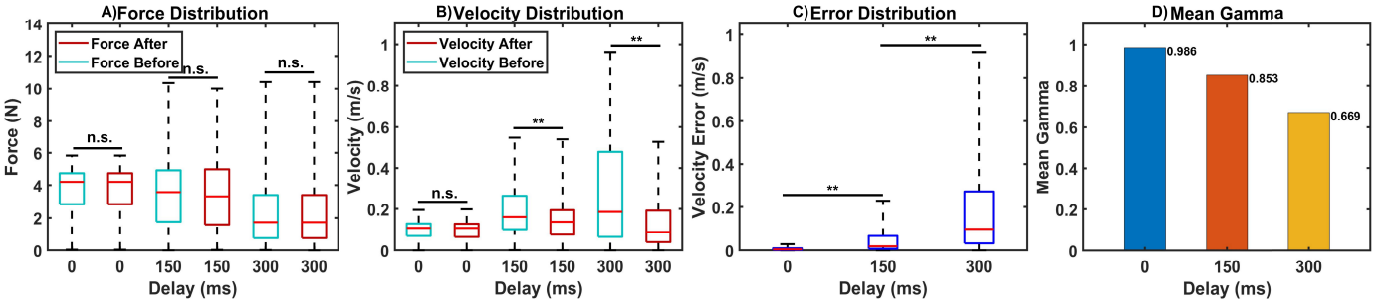

Fig. 7: Box plot distributions of force (A), velocity (B), velocity error (C), and mean γ (D) for Trial 1.

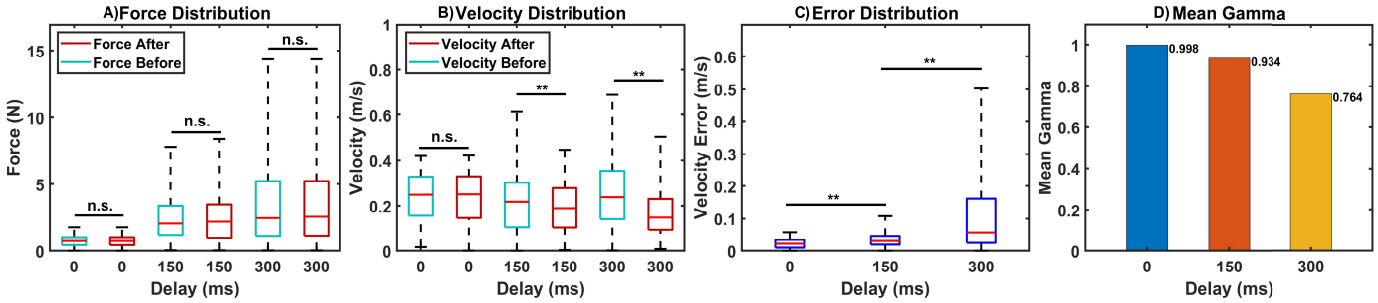

Fig. 8: Box plot distributions of force (A), velocity (B), velocity error (C), and mean γ (D) for Trial 2.

shows that the amount of modification increases as delays increases, which is due to the excessive non-passive energy which is injected into the network, which would challenge the stability if the proposed stabilizer was not in the loop. However, due to the adaptive and autonomous activation of the proposed stabilizer, which observes and governs the flow of non-passive energy, just enough dissipation is injected to balance the energy and guarantee stability. Fig. 7(D) and Fig. 8(D) show the mean γ (velocity modification parameter) at different delay values. The mean γ value trends downwards as the delay increases. Please note that lower γ means lower loop gain and thus higher velocity modulation.

D. Experimental Results - Trial 3

In this section, the experimental validation of the variable delay condition is shown. In addition, the performance of the proposed stabilizer is compared with the wave variable with wave scaling and filtering controller (see [8] for details on implementation). A wave impedance value of $b - 5$ was chosen to maximize the force transparency to create an agreeable comparison with the proposed stabilizer. Resistive and assistive interactions are conducted by the users from the first experiment with a variable delay of $\tau = 150 + 100\sin(5t)$ms. The scaling factor $g = 0.707$ was chosen based on the formulation of wave variable with scaling i.e., $g \leq \sqrt{1-\dot{\tau}}$ where $\dot{\tau}_{max} = 0.5$.

•Proposed Stabilizer (PV-VSPSC)

Fig. 9 shows the force, velocity, γ, and delay profiles during resistive interaction with the variable delay condition for the proposed stabilizer. It is shown that the leader-side forces and the reflected forces are tracked with minimal added deviation by the stabilizer. Again, this is expected since the stabilizer does not theoretically modify the force feedback to maximize force transparency as designed. Regarding the velocity tracking, it should be noted that the amount of modification increases due to the challenge to the system passivity, which can be seen in the γ profile. This shows that the stabilizer properly modifies the velocity, taking into account the follower-side user's EoP, to ensure that the passivity of the closed-loop system is preserved. The variable time delay profile is shown in Fig. 9.

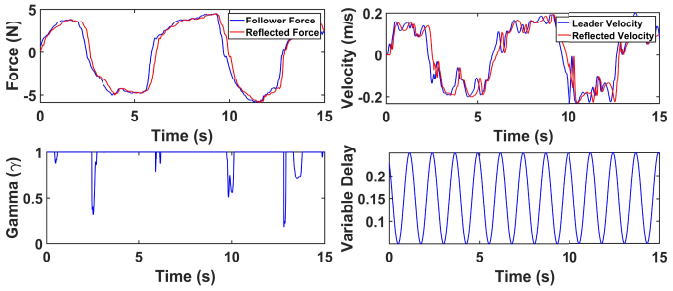

Fig. 9: Force, Velocity, γ, and Delay profiles during resistive interaction with variable delay using the proposed controller.

Fig. 10 shows the force, velocity, γ, and delay profiles during assistive interaction with the variable delay condition for the proposed stabilizer. Again, the leader-side forces and reflected forces are tracked with minimal added deviation by the stabilizer. The amount of velocity modification increases to ensure that the system remains passive. These experiments show the capability of the proposed PV-VSPSC velocity modification scheme to account for the EoP of the follower-side user to ensure that the passivity condition is thoroughly met in variable delay conditions and non-passive interactions.

•Wave Variable

Fig. 11 shows the force, velocity, and delay profiles during resistive and assistive interaction for the wave variable controller. The force profile shows the force sent from the follower side (blue) and the force reflected to the leader side (red). The

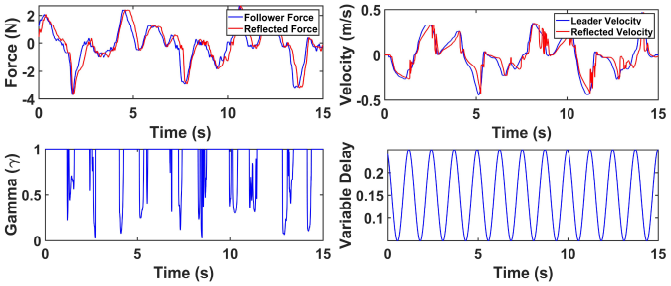

Fig. 10: Force, Velocity, γ, and Delay profiles during assistive interaction with variable delay using the proposed stabilizer.

velocity profile shows the velocity sent from the leader side (blue) and the velocity reflected to the follower side (red). At the chosen wave impedance, there is high performance in force tracking during resistive interactions. However, the force tracking performance during assistive interactions is poor. As can be seen during resistive interaction, the velocity tracking deteriorates when the force tracking improves. Likewise, when the force tracking deteriorates, the velocity tracking improves, as can be seen in the assistive interaction (this is a property of the wave variable method). The variable time delay can be seen in the delay plots.

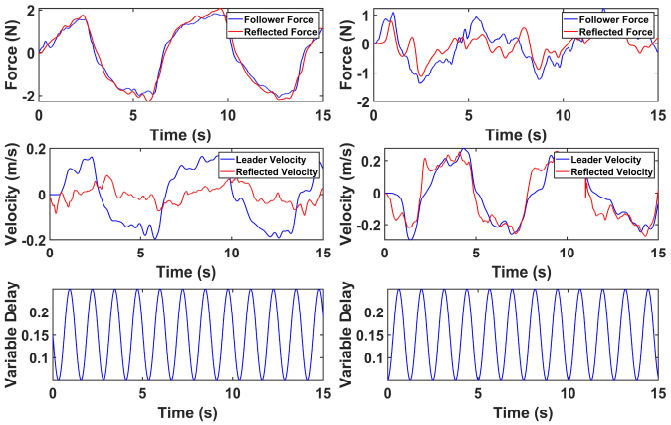

Fig. 11: Force, Velocity, and Delay profiles during resistive (left) interaction and assistive (right) interaction with variable delay using wave variable.

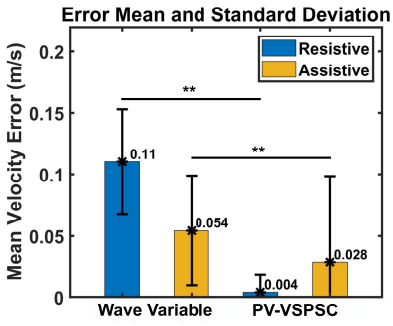

Fig. 12: Velocity Error for wave variable and proposed PV-VSPSC during resistive and assistive interactions.

To compare the results of the two controllers, the mean velocity error between the velocity sent from the leader-side and the velocity reflected to the follower side is shown in Fig. 12. The Wilcoxon non-parametric sign rank test is used

TABLE I

Variable	Value
Y_{th}	1/60 m/(N.s)
$f_p(t)^*$	chirp signal with a) initial freq = 0.1 Hz, b) Target Time = 15s and final freq = 4Hz
$v_{th}(t)^*$	chirp signal with a) initial freq = 0.5 Hz, b) Target Time = 15s and final freq = 10Hz
Z_p	$\in [10, 110]$ N.s/m
delay	$\in [0, 200] ms$ with a step size of 20 ms
Simulation time	15s

to compare the error distributions between the two controllers during resistive interactions and assistive interactions. There is a significant reduction in the velocity error using the proposed PV-VSPSC design compared to the wave variable method ($p < 0.001$). This is because the proposed design utilizes the knowledge of the follower side user's EoP to minimally modify the velocity. This shows the superiority of the proposed stabilizer when compared to the wave variable with the wave scaling method.

E. Simulation Results

While the conventional stabilizers in bilateral teleoperation (such as TDPC and M-TDPC) modify reflected force to the patient, the proposed stabilizer is designed to modify the velocity received by the therapist to block non-passivity and thus stabilize the system. The grid simulations are performed to draw observations and conclusions about the performance of the proposed stabilizer in a systematic manner for a wide range of parameters. Four different evaluation metrics have been considered for the grid study, namely: 1) Spearman correlation, 2) Root Mean Square Error, 3) Reflected Admittance, and 4) Energy Ratio. These parameters have been plotted against the patient impedance - Z_p (N.s/m) and delay (seconds) in a 3D plot for different estimates of therapist EoP. The mean γ value associated with each simulation is also evaluated.

As mentioned before, to design PV-VSPSC the therapist's motion is decomposed into active (v_{th}^*) and reactive components ($v_{th-react}$) where the reactive component, which represents the therapist's biomechanics ($v_{th-react} = Y_{th}(f_{th}, t)$), is considered to be passive while the restriction on passivity of the patient can be relaxed. This means that although the therapist admittance is passive in nature i.e $Y_{th} \in [0, \infty)$ the active component, v_{th}^* can still induce non-passive energies.

Here, a grid study is conducted to evaluate the performance of the stabilizer for various values of delays and patient impedances. The information regarding the variable values and ranges used for the grid simulation of the PV-VSPSC in a bilateral teleoperation architecture are presented in table I. The grid study is conducted with the patient impedance ranging from 10 N.s/m to 110 N.s/m, motivated by the results in the literature [43] and our previous work. In addition, regular internet delay ranging from 0 to 200 ms can be considered as a realistic number for within-country communication [1]–[4]. The simulation time for each simulation is 15 seconds.

The surface plots for various values of the estimated EoP are presented in Fig. 13 to Fig. 16 in different colors, as indicated by the legend. For example, the cyan surface plot corresponds to a simulation setting, which considers the highest estimate

of therapist admittance at 95% of Y_{th}, and the green surface plot corresponds to the simulation setting, which considers the most conservative estimate at 10% of Y_{th}. The following observations have been made for each metric:

Spearman Correlation: Fig. 13 displays the Spearman's correlation coefficient between velocity sent across the communication channel from the patient to the therapist v_{th} and the velocity reflected to the therapist by the stabilizer after modulation by the stabilizer, v_{th-mod}. Spearman's correlation coefficient measures a monotonic relationship between two variables. A value close to 1 indicates a strong monotonic (linear or nonlinear) association, and as the value gets closer to zero, it indicates a weak monotonic association. As can be seen in the result, since the teleoperation system is perfectly transparent for zero delays, Spearman's coefficient between the therapist velocity before and after the stabilizer is close to unity since the stabilizer does not modify the incoming velocities. For higher values of delay, a lower Spearman's coefficient is observed. Also, the coefficient decreases as the estimate of EoP becomes more conservative (which can be seen by comparing different colored surfaces). This is expected since the amplitude of the therapist velocity is reduced more by the stabilizer as the estimate of EoP becomes more conservative. The coefficient also decreases as the patient impedance Z_p is lowered from 60 Ns/m because below this value $Z_p < Z_{th}$. A noticeable drop in the Spearman Correlation Coefficient is observed between 0 ms delay and 0.025 ms delay. Since the stabilizer is implemented in a fully transparent system, which has been shown to be on the edge of stability, the minimum additional delay beyond 0 would make the system non-passive and, in the case of no stabilizer, unstable. Therefore, this results in activation of the stabilizer and a drop in the Pearson Correlation Coefficient, and an increase in the RMSE.

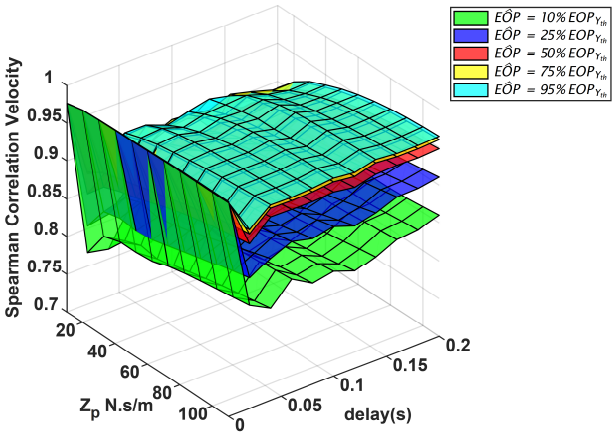

Fig. 13: Spearman correlation between the therapist velocity before the stabilizer (v_{th}) and after the stabilizer v_{th-mod}

Reflected admittance to the therapist: The generated therapeutic behavior ($D_{therapy}$), which represents the extent of energy delivered from the patient to the therapist in the teleoperation system and felt by the therapist, is calculated as:

$$D_{therapy} = \frac{\int_0^t f_{th}(t)^T . v_{th-mod}(t)}{\int_0^t f_{th}^T(t) . f_{th}(t)} \tag{15}$$

It should be noted that $D_{therapy}$ is an admittance-based calculation. Fig. 14 displays a grid study of the admittance-based passivity reflected to and felt by the therapist, $D_{therapy}$, for various values of patient impedance and delay. It can be observed that the admittance felt by the therapist caps at a max value which is equal to the considered estimate of the therapist's EoP. The stabilizer has achieved this by compensating only for the non-passive energies that cannot be handled by the therapist's biomechanics and reflecting the remaining energy to the patient, even for a conservative estimate of the therapist's EoP which can be concluded by observing the surface plots for the various EoP estimates indicated by the legend.

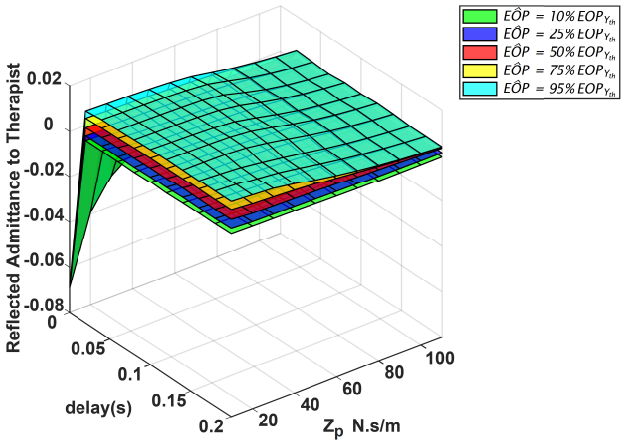

Fig. 14: Admittance reflected to and felt by the therapist

Root Mean Square Error (RMSE): Root Mean Square Error (RMSE) is a measure of the deviation between the velocity reflected to the therapist from the patient across the communication channel v_{th} and the therapist velocity after modification by the stabilizer v_{th-mod}:

$$RMSE = \sqrt{\sum_{i=1}^{n} \frac{(v_{th}(i) - v_{th-mod}(i))^2}{n}} \tag{16}$$

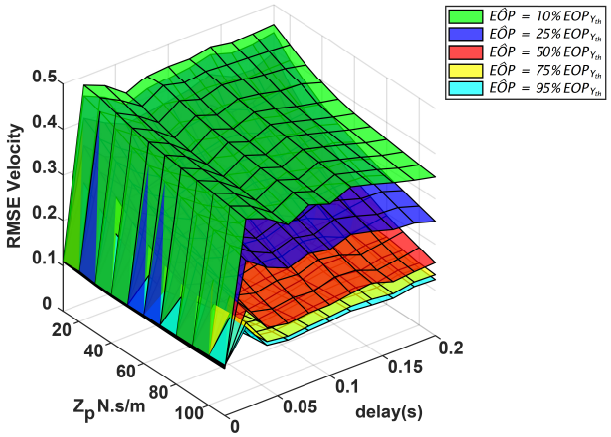

Fig. 15: RMSE between therapist velocity before and after the stabilizer

The RMSE is expected to be higher as the EoP estimate becomes more conservative due to a higher reduction in the

amplitude of the therapist velocity by the stabilizer to compensate for the excess system energy based on the estimated EoP of the therapist. The same can be confirmed from the surface plots for different EoP estimates in Fig.15. Additionally, the RMSE decreases as the patient impedance Z_p increases for a given EoP Estimate, as this will enhance the stability margin, which is noted autonomously by the stabilizer. The noticeable rise in the RMSE values between 0 ms and 0.025 ms delay is attributed to the same reason mentioned for the Spearman Correlation Coefficient.

Energy Ratio - E_{th-mod}/E_{th} **:** Fig. 16 displays the surface plots of the ratio of the energy at the therapy terminal after the stabilizer to the energy before the stabilizer. A value close to one indicates that the stabilizer reflected most of the energy to the therapist without modification. A lower ratio indicates that the stabilizer acts as a gate and only lets a certain portion of the incoming energy to pass through.

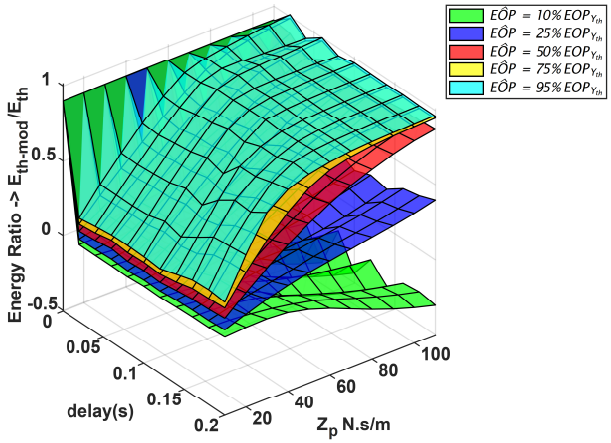

Fig. 16: Energy Ratio

It can be observed that the ratio is higher for estimates of EoP closer to the actual therapist admittance. This is because the stabilizer modifies the velocity based on the real-time estimates of the EoP of the therapist's biomechanics. The ratio is close to unity for zero delays for all Z_p since at zero delays, the implemented two-channel teleoperation system is theoretically transparent and stable. This is autonomously noted by the stabilizer, and minimal-to-no energy modification is observed. For higher values of delay, energy modification is more significant, and the behavior of the stabilizer depends on the conservatism of the EoP estimates (which is a novel degree of flexibility proposed in this work for PV-VSPSC). It can therefore be said that instead of blocking all active energies flowing in the system, the proposed nonlinear variable structure stabilizer is able to automatically modulate the behavior based on the estimated absorption capability of the therapist and only blocks the instability-inducing components of the energy, which cannot be counteracted or balanced by the inherent biomechanical EoP.

Mean Gamma Value (γ) **:** Fig. 17 shows the surface plots of the mean γ values of the stabilizer. A mean γ value close to unity indicates that the stabilizer was minimally active. A value close to zero indicates that the stabilizer was very active.

These results follow closely with the energy ratio results supporting that the stabilizer is active when the delay is non-

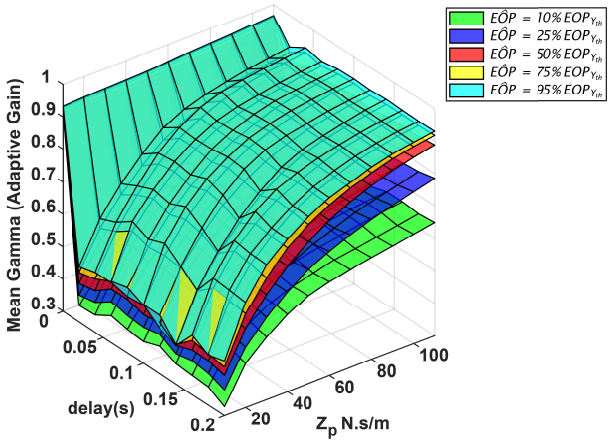

Fig. 17: Mean Gamma

zero and at lower estimates of EoP. The results support the proposed design and show the flexibility of the stabilizer in response to the changes in the delay and estimates of the EoP.

IV. Conclusion

This paper introduces an admittance-based power-domain velocity modulation design for the proposed VSPSC stabilizer that is focused on the application of telerehabilitation. The stabilizer observes the energy at the therapy terminal and utilizes the extrapolation of biomechanical EoP to calculate energy absorption and modulate the flow of energy in a customized manner. The EoP is estimated by measuring the grasping pressure (representative of co-contraction) in real-time and mapping it to the EoP map generated offline and fed to the stabilization algorithm of the proposed nonlinear adaptive stabilizer. If the passivity of the user's biomechanics can compensate for the instability-inducing components, the stabilizer allows for the velocity to be directly reflected to the therapist without modification. Otherwise, the stabilizer autonomously intervenes and modulates the velocity that is sent from the patient across the communication to the therapist to stabilize the system. This paper, for the first time, proposes an EoP-based velocity domain variable structure passivity control algorithm that can guarantee stability while taking into account the inherent sources of energy absorption to enhance transparency. Although the work was motivated and designed for telerobotic rehabilitation, it can be used for several other applications, including human-centered teleoperation, hand-over-hand surgical training, mirror rehabilitation, and haptic communication. The future work involves evaluating the proposed telerobotic system in applied environments such as telerehabilitation. This study does not include a usability analysis of patients in clinical settings. This is one of the limitations of the current study, which will be the focus of our future work.

References

[1] S. F. Atashzar *et al.*, "Haptics-enabled interactive neurorehabilitation mechatronics: Classification, functionality, challenges and ongoing research," *Mechatronics*, vol. 57, pp. 1–19, 02 2019.

[2] S. Mehrdad *et al.*, "Review of Advanced Medical Telerobots," *Applied Sciences*, vol. 11, no. 1, p. 209, Dec. 2020. [Online]. Available: https://hal.archives-ouvertes.fr/hal-03102790

[3] N. Feizi *et al.*, "Robotics and ai for teleoperation, tele-assessment, and tele-training for surgery in the era of covid-19: Existing challenges, and future vision," *Frontiers in Robotics and AI*, vol. 8, 2021.

[4] S. Atashzar *et al.*, "Review: How can intelligent robots and smart mechatronic modules facilitate remote assessment, assistance, and rehabilitation for isolated adults with neuro-musculoskeletal conditions?" *Frontiers in Robotics and AI*, vol. 8, Apr. 2021.

[5] R. J. Anderson and M. W. Spong, "Bilateral control of teleoperators with time delay," *IEEE Transactions on Automatic control*, vol. 34, no. 5, pp. 494–501, 1989.

[6] G. Niemeyer and J. . E. Slotine, "Stable adaptive teleoperation," *IEEE Journal of Oceanic Engineering*, vol. 16, no. 1, pp. 152–162, 1991.

[7] D. Sun *et al.*, "Wave-variable-based passivity control of four-channel nonlinear bilateral teleoperation system under time delays," *IEEE/ASME Transactions on Mechatronics*, vol. 21, no. 1, pp. 238–253, 2016.

[8] R. Lozano *et al.*, "Passivation of force reflecting bilateral teleoperators with time varying delay," in *in Proceedings of the 8. Mechatronics Forum*, 2002, pp. 24–26.

[9] C. Yang *et al.*, "Teleoperation control based on combination of wave variable and neural networks," *IEEE Transactions on Systems, Man, and Cybernetics: Systems*, vol. 47, no. 8, pp. 2125–2136, 2017.

[10] Jee-Hwan Ryu *et al.*, "Stable teleoperation with time-domain passivity control," *IEEE Transactions on Robotics and Automation*, vol. 20, no. 2, pp. 365–373, 2004.

[11] J. Artigas *et al.*, "Time domain passivity control for position-position teleoperation architectures," *Presence*, vol. 19, no. 5, pp. 482–497, 2010.

[12] Y. Ye *et al.*, "A power-based time domain passivity control for haptic interfaces," *IEEE Transactions on Control Systems Technology*, vol. 19, no. 4, pp. 874–883, 2011.

[13] Y. Ye *et al.*, "Bilateral teleoperation with time-varying delay: A communication channel passification approach," *IEEE/ASME Transactions on Mechatronics*, vol. 18, no. 4, pp. 1431–1434, 2013.

[14] J. Rebelo and A. Schiele, "Time domain passivity controller for 4-channel time-delay bilateral teleoperation," *IEEE Transactions on Haptics*, vol. 8, no. 1, pp. 79–89, 2015.

[15] S. Liu *et al.*, "A four-channel time domain passivity approach for bilateral teleoperator," in *2018 IEEE International Conference on Mechatronics and Automation (ICMA)*. IEEE, 2018, pp. 318–322.

[16] V. Chawda *et al.*, "Compensating position drift in time domain passivity approach based teleoperation," in *2014 IEEE Haptics Symposium (HAPTICS)*, 2014, pp. 195–202.

[17] V. Chawda and M. K. O'Malley, "Position synchronization in bilateral teleoperation under time-varying communication delays," *IEEE/ASME Transactions on Mechatronics*, vol. 20, no. 1, pp. 245–253, 2014.

[18] U. Ahmad and Y. Pan, "A time domain passivity approach for asymmetric multilateral teleoperation system," *IEEE Access*, vol. 6, pp. 519–531, 2018.

[19] J.-H. Ryu *et al.*, "Multilateral teleoperation over communication time delay using the time-domain passivity approach," *IEEE Transactions on Control Systems Technology*, vol. 28, no. 6, pp. 2705–2712, 2020.

[20] D. Lee and K. Y. Lui, "Passive configuration decomposition and passivity-based control of nonholonomic mechanical systems," *IEEE Transactions on Robotics*, vol. 33, no. 2, pp. 281–297, 2017.

[21] M. De Stefano *et al.*, "A passivity-based approach for simulating satellite dynamics with robots: Discrete-time integration and time-delay compensation," *IEEE Transactions on Robotics*, vol. 36, no. 1, pp. 189–203, 2020.

[22] X. Xu *et al.*, "Energy prediction for teleoperation systems that combine the time domain passivity approach with perceptual deadband-based haptic data reduction," *IEEE Transactions on Haptics*, vol. 9, no. 4, pp. 560–573, 2016.

[23] H. Lee *et al.*, "Passivity controller based on load-side damping assignment for high stiffness controlled series elastic actuators," *IEEE Transactions on Industrial Electronics*, vol. 68, no. 1, pp. 871–881, 2021.

[24] A. Jafari *et al.*, "The input-to-state stable (iss) approach for stabilizing haptic interaction with virtual environments," *IEEE Transactions on Robotics*, vol. 33, no. 4, pp. 948–963, 2017.

[25] D. Heck *et al.*, "Direct force-reflecting two-layer approach for passive bilateral teleoperation with time delays," *IEEE Transactions on Robotics*, vol. 34, no. 1, pp. 194–206, 2018.

[26] C. Secchi *et al.*, "Position drift compensation in port-hamiltonian based telemanipulation," pp. 4211–4216, 2006.

[27] F. Ferraguti *et al.*, "Optimized power modulation in wave-based bilateral teleoperation," *IEEE/ASME Transactions on Mechatronics*, vol. 26, no. 1, pp. 276–287, 2021.

[28] C. Secchi and F. Ferraguti, "Energy optimization for a robust and flexible interaction control," in *2019 International Conference on Robotics and Automation (ICRA)*, 2019, pp. 1919–1925.

[29] B. Capelli *et al.*, "Passivity and control barrier functions: Optimizing the use of energy," *IEEE Robotics and Automation Letters*, vol. 7, no. 2, pp. 1356–1363, 2022.

[30] S. F. Atashzar *et al.*, "A passivity-based approach for stable patient–robot interaction in haptics-enabled rehabilitation systems: Modulated time-domain passivity control," *IEEE Transactions on Control Systems Technology*, vol. 25, no. 3, pp. 991–1006, 2017.

[31] S. F. Atashzar *et al.*, "A grasp-based passivity signature for haptics-enabled human-robot interaction: Application to design of a new safety mechanism for robotic rehabilitation," *The International Journal of Robotics Research*, 04 2017.

[32] S. Thudi and S. F. Atashzar, "Discrete windowed-energy variable structure passivity signature control for physical human-(tele)robot interaction," *IEEE Robotics and Automation Letters*, vol. 6, no. 2, pp. 3647–3654, 2021.

[33] S. F. Atashzar *et al.*, "Energetic passivity decoding of human hip joint for physical human-robot interaction," *IEEE Robotics and Automation Letters*, vol. 5, no. 4, pp. 5953–5960, 2020.

[34] S. F. Atashzar *et al.*, "Control of time-delayed telerobotic systems with flexible-link slave manipulators," in *2012 IEEE/RSJ International Conference on Intelligent Robots and Systems*, 2012, pp. 3035–3040.

[35] S. F. Atashzar *et al.*, "A small-gain approach for nonpassive bilateral telerobotic rehabilitation: Stability analysis and controller synthesis," *IEEE Transactions on Robotics*, vol. 33, no. 1, pp. 49–66, 2017.

[36] D. B. Gandhi *et al.*, "Mirror therapy in stroke rehabilitation: Current perspectives," *Therapeutics and Clinical Risk Management*, vol. 16, pp. 75 – 85, 2020.

[37] J. Xu *et al.*, "A multi-channel reinforcement learning framework for robotic mirror therapy," *IEEE Robotics and Automation Letters*, vol. 5, no. 4, pp. 5385–5392, 2020.

[38] M. Shahbazi *et al.*, "Robotics-assisted mirror rehabilitation therapy: A therapist-in-the-loop assist-as-needed architecture," *IEEE/ASME Transactions on Mechatronics*, vol. 21, no. 4, pp. 1954–1965, 2016.

[39] M. Shahbazi *et al.*, "Multimodal sensorimotor integration for expert-in-the-loop telerobotic surgical training," *IEEE Transactions on Robotics*, vol. 34, no. 6, pp. 1549–1564, 2018.

[40] F. Liu *et al.*, "An energy-based approach for n-d.o.f. passive dual-user haptic training systems," *Robotica*, vol. 38, no. 7, p. 1155–1175, 2020.

[41] E. Ivanova *et al.*, "Short time delay does not hinder haptic communication benefits," *IEEE Transactions on Haptics*, vol. 14, pp. 322–327, 2021. [Online]. Available: http://dx.doi.org/10.1109/TOH.2021.3079227

[42] A. Takagi *et al.*, "Haptic communication between humans is tuned by the hard or soft mechanics of interaction," *PLOS Computational Biology*, vol. 14, no. 3, Mar 2018.

[43] T. Tsuji *et al.*, "Human hand impedance characteristics during maintained posture," *Biological cybernetics*, vol. 72, no. 6, pp. 475–485, 1995.

[44] L. Masia and V. Squeri, "A modular mechatronic device for arm stiffness estimation in human–robot interaction," *IEEE/ASME Transactions on Mechatronics*, vol. 20, no. 5, pp. 2053–2066, 2014.

[45] M. Dyck and M. Tavakoli, "Measuring the dynamic impedance of the human arm without a force sensor," in *2013 IEEE 13th International Conference on Rehabilitation Robotics (ICORR)*. IEEE, 2013, pp. 1–8.

[46] P. H. McCrea *et al.*, "Linear spring damper model of the hypertonic elbow: reliability and validity," *Journal of neuroscience methods*, vol. 128, no. 1-2, pp. 121–128, 2003.

[47] M. Vidyasagar, *Nonlinear systems analysis*. SIAM, 2002.

[48] J. R. Forbes and C. J. Damaren, "Passive linear time-varying systems: State-space realizations, stability in feedback, and controller synthesis," in *Proceedings of the 2010 American Control Conference*. IEEE, 2010, pp. 1097–1104.

[49] G. Herrnstadt and C. Menon, "Voluntary-driven elbow orthosis with speed-controlled tremor suppression," *Frontiers in Bioengineering and Biotechnology*, vol. 4, 03 2016.

[50] B. Taheri *et al.*, "Adaptive suppression of severe pathological tremor by torque estimation method," *IEEE/ASME Transactions on Mechatronics*, vol. 20, no. 2, pp. 717–727, 2015.

Peter Paik (Student Member, IEEE) received the B.Sc degree in mechanical engineering in 2020 and the M.Sc degree in robotics in 2022 from New York University (NYU), New York, NY, USA. He is working toward his Ph.D. under the supervision of Prof. S. Farokh Atashzar in robotics at the Department of Electrical and Computer Engineering, NYU, New York, NY, USA. At NYU, he is a researcher at the Medical Robotics and Interactive Intelligent Technologies (MERIIT) Laboratory, and his research interests include human-centered robotics, human-machine interaction, and medical robotics.

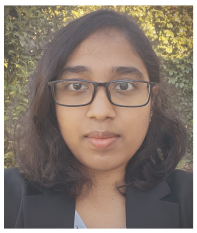

Smrithi Thudi received her B.Tech degree in Mechatronics Engineering from Manipal Institute of Technology, Manipal, Karnataka, India, in 2018 and a Master's degree in Mechatronics and Robotics from New York University (NYU), New York, NY, USA, in 2021. At NYU, she conducted research under the supervision of Prof. S. Farokh Atashzar. She is currently working as a Mechatronics Engineer at Motivo Engineering, Gardena, CA, USA. Her research interests include human-robot interactions, rehabilitation robotics, haptics, and control systems.

S.Farokh Atashzar (Senior Member, IEEE) received his Ph.D. degree in electrical and computer engineering from the University of Western Ontario, London, ON, Canada, in 2017. He is currently an Assistant Professor with New York University (NYU), New York, NY, USA, jointly appointed with the Department of Electrical and Computer Engineering and the Department of Mechanical and Aerospace Engineering. He is also affiliated with the department of Biomedical Engineering at NYU (New York, NY, USA), also, NYU WIRELESS (New York, NY, USA), and NYU Center for Urban Science and Progress (New York, NY, USA). Before joining NYU, he was a Postdoctoral Scientist with Imperial College London, London, UK. At NYU, he is the director of the Medical Robotics and Interactive Intelligent Technologies (MERIIT) Lab. The lab is mainly funded by the US National Science Foundation. His research interests include a human-machine interface, human-centered robotics, neural interfacing, deep learning, and nonlinear control. Prof. Atashzar was the recipient of several awards, including the 2021 Outstanding Associate Editor of the IEEE ROBOTICS AND AUTOMATION LETTERS. He is currently an Associate Editor for the IEEE TRANSACTIONS ON ROBOTICS and IEEE ROBOTICS AND AUTOMATION LETTERS.